ILASS–Europe 2022, 31th Conference on Liquid Atomization and Spray Systems, 6-8 September 2022, Virtual, Israel

Impact of the Mixing Chamber Geometry of a Y-jet Atomizer on Atomization Efficiency and Spray Characteristics

Matheus Rover Barbieri*[1], Artur Karlin[1], Lydia Achelis[1], Udo Fritsching[1,2]
[1]Particles and Process Engineering Department, Faculty of Production Engineering, Universität Bremen, Bibliothekstr. 1, 28359 Bremen, Germany
[2]Leibniz Institute for Materials Engineering IWT, Badgasteiner Str. 3, 28359 Bremen, Germany
*Corresponding author: m.barbieri@iwt.uni-bremen.de

Abstract

A specific design of internal-mixing twin-fluid atomizers is the Y-jet nozzle, in which the liquid and the gas jets impinge inside the mixing chamber with a specific angle between them. Some geometrical configurations are explored to promote an effective momentum transfer between the fluids. Hence, this work aims to improve the atomization efficiency by proposing modifications to the internal-mixing chamber of Y-jet atomizers. For this, experimental measurements employing the phase-Doppler anemometry (PDA) technique are conducted using water and air. Given a base geometry, the design variations consider increasing the length and the opening angle of the mixing chamber. Measurement results axially distributed from 65 to 145 mm downstream of the nozzle outlet indicate a strong dependence of the spray droplet statistics on both the mixing chamber length and opening angle. Shorter mixing chamber lengths promote higher atomization efficiencies at the evaluated operating condition.

Keywords

Internal-mixing nozzle, Nozzle geometry, Spray instabilities, Droplet sizes and velocities

Introduction

Twin-fluid atomizers are widely used in several applications, especially when dealing with viscous and complex rheology fluids, such as in rocket engines, and in fluid catalytic cracking units in the oil refineries, where the raw oil is atomized using steam as the dispersing medium [5][7]. Internal-mixing atomizers promote the first contact between the gas and the liquid in a chamber inside the nozzle, ensuring a more intense contact between the fluids and an enhanced momentum transfer from the high-speed gas jet to the liquid stream [3][4].

A special configuration of internal-mixing atomizers is the Y-jet design [2][10], in which the liquid and the gas jets impinge inside the mixing chamber at a specific angle. In this context, numerous geometrical configurations are explored to promote a more effective mixing and momentum transfer between the fluids, leading to a better atomization performance. Several studies have addressed numerical [9] and experimental [1][8][10][12] analyses of the effect of changing the nozzle geometry mainly on droplet sizes and velocities.

Although several mixing-chamber geometric features have been investigated, they are usually dissociated from the spatial distribution of droplet sizes and velocities, especially when dealing with high mass flow rates, and only a few address the impacts of geometric changes over the atomization performance. From this perspective, the present work aims to improve the atomization efficiency of Y-jet atomizers by proposing geometric modifications to the internal-mixing chamber.

A specific design of the Y-jet atomizer is therefore investigated. It consists of two angled liquid jets positioned 180° apart being disrupted by a high-speed central gas jet coming from above. The three jets impinge inside a conical chamber before leaving the nozzle. Based on

this fundamental design, the investigation focuses on the internal-mixing chamber length and its opening angle, which are also associated with the mixing chamber outlet diameter, using water and air as working fluids. Droplet size and velocity distributions at different axial positions are simultaneously measured with a phase-Doppler anemometer, and the efficiency of each atomizer is computed based on the liquid and gas necessary power to increase the liquid surface energy.

Materials and Methods

The study utilizes an experimental facility using water and air as working fluids. The liquid is stored in a tank under the spray chamber and from there pumped to the nozzle by a centrifugal pump. The liquid mass flow rate is measured by a flow meter (OPTISONIC 3400 C from Krohne) and the liquid pressure by a pressure sensor (PT5404 from IFM). The compressed air is supplied by a central supply at room temperature (23±2°C). Before reaching the nozzle, it passes a flow meter (OPTISWIRL 4200 from Krohne) and a pressure sensor (PI2204 from IFM). Thermocouples (of NiCr-Ni from company TMH, with a range of -200 to 1300°C) are also included in the liquid and gas lines. The spray is formed inside a closed cylindrical-shaped chamber with 60 cm of diameter and a height of 140 cm. The liquid is collected in the tank below the chamber to be again pumped to the nozzle. The data of the mass flow rate, pressure, and temperature sensors are stored and monitored from a computer with LabVIEW. Control parameters of the experiments are the pumping rate and the gas pressure, both adjusted from the computer.

The length and opening angle of the internal mixing chamber are the geometrical parameters investigated in the present work. For that, three nozzles are available varying these design features according to **Figure 1**.

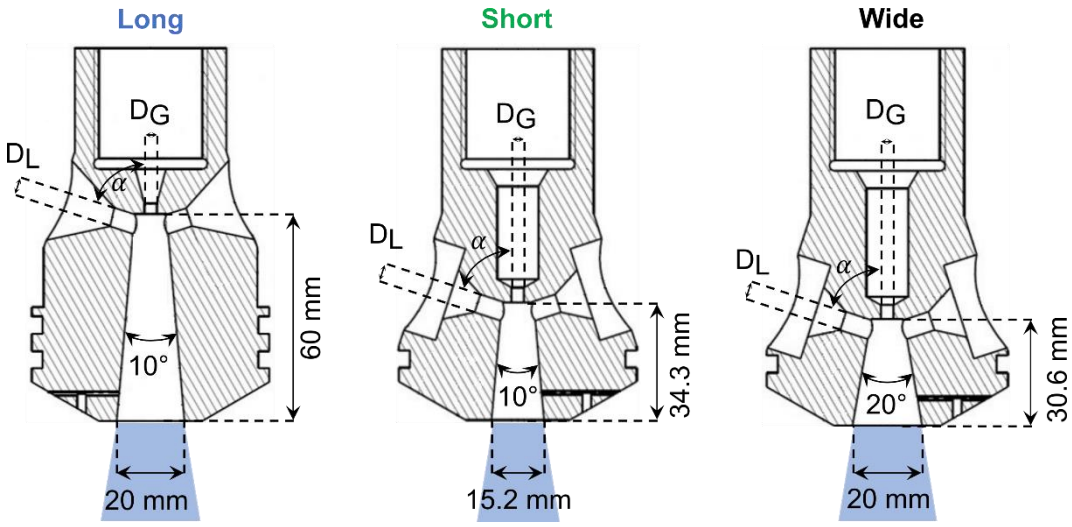

Figure 1. Nozzle geometries with the respective dimensions. D_L = 5.5 mm and D_G = 3.6 mm.

The “Long” nozzle has the longest mixing chamber (60 mm) and an opening angle of 10°, resulting in a mixing-chamber outlet diameter of 20 mm. The “Short” nozzle has about half of the internal-mixing chamber length (34.3 mm) and an opening angle of 10°, presenting also the narrowest mixing chamber exit diameter (15.2 mm). The “Wide” geometry consists of keeping a similar mixing chamber length (30.6 mm) of the “Short” nozzle and the double the opening angle (20°). It has the same outlet diameter as the “Long” geometry. The air supply channel (with minimal diameter D_G = 3.6 mm) and the two angled water channels (with minimal

diameter D_L = 5.5 mm) are unchanged, as well as the impingement angle between them (α = 72°).

Droplet size and velocity data are simultaneously acquired with a phase-Doppler anemometer (BSA 6000, Dantec Dynamics A/S, Tonsbakken, Denmark). At each measuring point, 20000 samples for computing the mean axial velocity and the Sauter mean diameter (SMD) are taken. The experiments are repeated three times for each measuring point. An argon-ion laser is used to generate green laser beams at 532-nm wavelength. The focal length of the emitting optics is 750 mm, while the focal length of the receiving optics is 1000 mm. A detection angle of 30 ° is used to acquire the first-order refracted light.

At 5 measuring points the droplet sizes and velocities are measured at axial distances from 65 to 145 mm at the spray centerline, spaced 20 mm apart. A region close to the nozzle is investigated, where the breakup and coalescence effects are still effective and are necessary to understand the atomization process and the instabilities which lead to the spray development. The operating condition practiced in the present work for each nozzle consists of absolute air pressure of 7 bar and a constant liquid mass flow rate of 2210.76$\pm$13.04 kg/h. Due to the different mixing chamber geometries, different discharge coefficients are expected in each nozzle, resulting in slightly different air mass flow rates and gas-to-liquid mass flow rate ratios, as presented in **Table 1**.

Table 1 - Air mass flow rate for each nozzle and the respective gas-to-liquid ratio (GLR)

	Nozzle		
	Long	Small	Wide
Air mass flow rate (kg/h)	43.71±0.66	40.80±0.82	46.42±2.76
GLR	0.020	0.018	0.021

The investigation of the nozzle design is a key parameter in the atomization performance, directly affecting the efficiency of the process. Effective atomization is paramount for a good mixing between the gas and liquid phases, enabling better control of the process. In this context, the atomization efficiency is usually computed considering the increase of the liquid's surface area, in which the droplet size plays a very important role.

The efficiency of an atomizer (ϵ) is calculated as the ratio of the power to increase the liquid surface energy (E_σ) to the power required to drive the liquid and the atomizing gas through the nozzle (E_0), defined by Eq. (1):

$$\epsilon = \frac{E_\sigma}{E_0}. \tag{1}$$

The power for the generation of spray surface energy (E_σ) is calculated using Eq. (2) [11]:

$$E_\sigma = \frac{6 Q_L \sigma}{SMD}, \tag{2}$$

where Q_L is the liquid volumetric flow rate (m³/s).

For internal-mixing designs, the power for driving the liquid and atomizing gas through the nozzle (E_0) is computed by two terms: one accounting for the power necessary to isothermally compress the gas (E_G) and the contribution of the pumping power of the liquid (E_L), considered for nozzles operated at low gas-to-liquid ratios [11], which are calculated as:

$$E_0 = E_G + E_L = \dot{m}_G R T ln\left(\frac{p_{G,abs}}{p_{G,0}}\right) + p_L Q_L, \tag{3}$$

where $\dot{m}_G$ is the gas mass flow rate (kg/s), R is the gas constant for air (J/(kg K)), T is the air temperature (K), $p_{G,abs}$ is the absolute gas pressure being injected into the atomizer, $p_{G,0}$ is the air pressure at atmospheric conditions, and p_L is the pressure of the liquid being injected into the nozzle.

Results and Discussion

The axial variation of the droplet's mean axial velocity and Sauter mean diameter for the three nozzles at the spray centerline is shown in **Figure 2(a)** and **Figure 2(b)**, respectively. Each marker represents the average and the error bar at each position is the standard deviation over three measurements. The mean axial velocity in **Figure 2(a)** showed a similar behavior between the three nozzles with a slight reduction with the axial position (maximum reduction of 4.72% for the nozzle Long). The differences are observed in the velocity magnitude, being attributed to the distinct geometries, especially to the nozzles' distinct opening angles. A remarkable lower spray velocity is promoted by the Wide nozzle (average of 36.5 m/s), which is about 66% of the spray velocity obtained with the Short nozzle. From **Figure 2(a)** it can also be inferred that longer mixing chambers reduce the efficacy of the momentum transfer from the gas to the liquid, indicated by the lower velocities achieved by the spray with the Long nozzle in comparison to the Short nozzle. This may be attributed to the pressure drop caused by the longer path for the gas-liquid mixture to flow inside the mixing chamber.

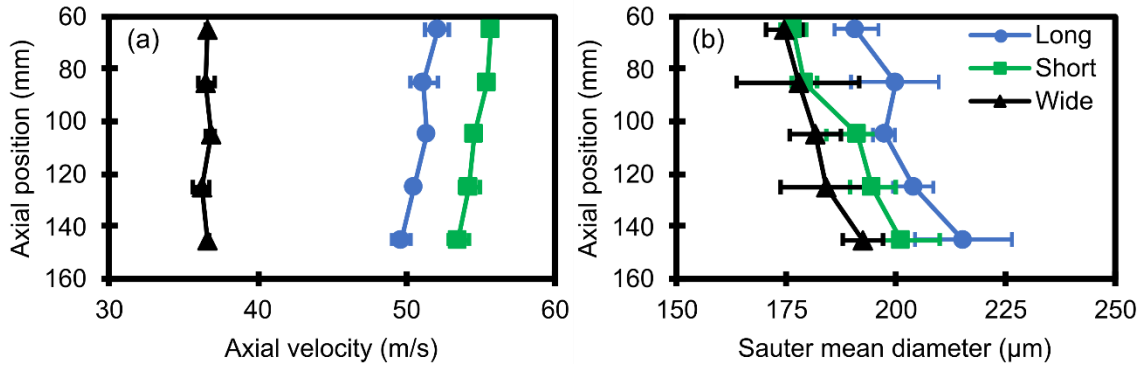

Figure 2. Axial variation of (a) mean axial velocity and (b) Sauter mean diameter for the three nozzles.

The behavior of the spray axial velocities is also associated with the droplet sizes' axial development as depicted in **Figure 2(b)**. A slight increase (maximum increase of 14% - from 176.4 μm to 201.1 μm – for the Short nozzle) is observed. While the mixing chamber with the wider opening angle yields smaller Sauter mean diameters, the larger drop sizes at all axial positions are produced by the nozzle Long. Therefore, it can be stated that not only the kinetic energy exchange between the high-speed gas stream and the liquid plays an important role in promoting the atomization, but also the instabilities triggered by the nozzle geometry are paramount for the liquid breakup. In this regard, further analyses about the atomization mechanisms and the development of the mixing status inside the atomization chamber are being carried out in subsequent studies.

As observed in **Figure 2**, the generation of smaller droplet sizes is, however, not associated with higher axial velocities. The kinetic energy of the gas phase can be directed toward two basic contributions in atomization. The first is to direct energy to the surface of the liquid,

causing instabilities that lead to its breakup into ligaments and droplets, while the second is to contribute to the kinetic energy of the liquid by accelerating it. The geometric configuration of the Wide nozzle, when operated under this operating condition, clearly induces the gas phase to promote a more efficient breakup of the droplets, rather than contributing to their velocity.

On the other hand, the Short nozzle achieves a better distribution of gas and liquid power for driving the liquid and atomizing gas through the nozzle. As can be seen in **Figure 2**, this nozzle produced the highest velocities in this operating condition and slightly larger droplets (axially averaged Sauter mean diameter of 188.45 µm) compared to the Wide nozzle (axially averaged Sauter mean diameter of 181.92 µm). The Long nozzle underperformed the Short nozzle concerning both droplet sizes and delivery of gas kinetic energy to the liquid, however, this distribution of gas energy was more balanced than the Wide nozzle. Thus, it is noted that the geometric configuration of the internal mixing chamber plays a key role not only in droplet generation but also in the liquid and gas power distribution on important parameters for atomization. These analyses can also be associated with the droplet size-velocity distributions in **Figure 3**. These plots are obtained as the average over every 50 detected drops (that have a priori been sorted by droplet diameter).

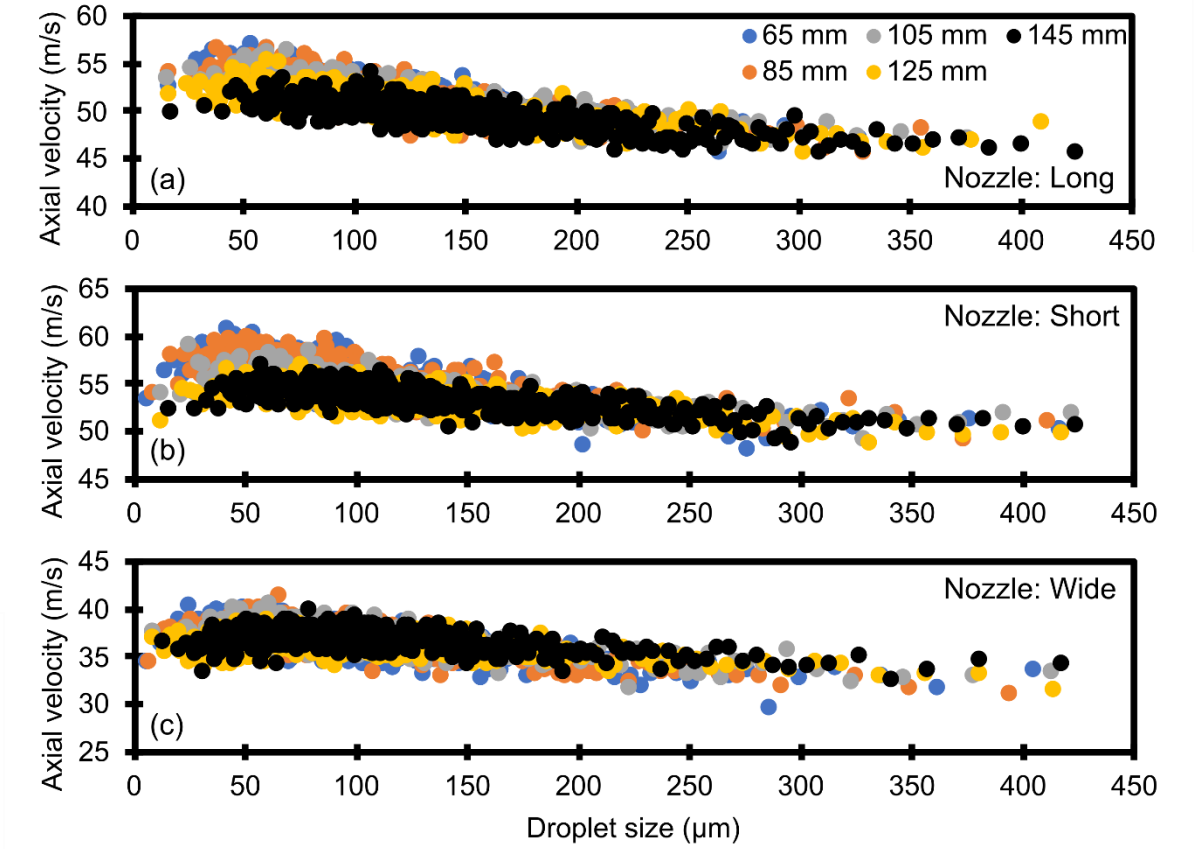

Figure 3. Droplet size-velocity correlation for different axial positions at the spray centerline for nozzle (a) Long, (b) Short, and (c) Wide.

The scatterplots confirm the trend already observed for the mean axial droplets' velocities. Especially for the Long and Short nozzles (**Figure 3(a)** and **Figure 3(b)**, respectively), there is a reduction in the droplets' axial velocity as the measuring point is moved away from the nozzle (for increasing axial distance). The droplet size-velocity plot for the Wide nozzle (**Figure**

3(c)), on the other hand, presents a similar velocity throughout the whole axial distance range investigated.

Furthermore, in regions closer to the nozzle outlet (at z = 65 and 85 mm, for instance), the scatterplots show a higher dependence of the droplets' velocities with their size. This is evidenced by a steeper velocity reduction as the drops' sizes increase. In other words, closer to the mixing chamber outlet, droplets within the size range up to 100 µm are more easily accelerated by the gas (due to their lower inertia) and reach higher velocities compared to larger droplets. As these liquid structures further develop and interact with themselves, an impingement effect can be inferred, in which upstream and higher-velocity droplets impinge on downstream and slower ones, leading to an exchange of kinetic energy. As the spray develops, the droplet velocities become more independent from their size, as can be seen for the axial position of 145 mm, for instance, where the size-velocity profiles are flattened and the variation of the droplet velocity with its size is not so steep.

The impingement of the small droplets with higher velocities (which are essentially found closer to the nozzle) with the downstream and lower-velocity droplets leads to an overall coalescence effect, as can be observed in the density distributions for the three nozzles in **Figure 4**. As the measuring point moves away from the nozzle outlet, there is a reduction of the small droplets fraction and an overall shift of the density distributions towards larger droplet sizes.

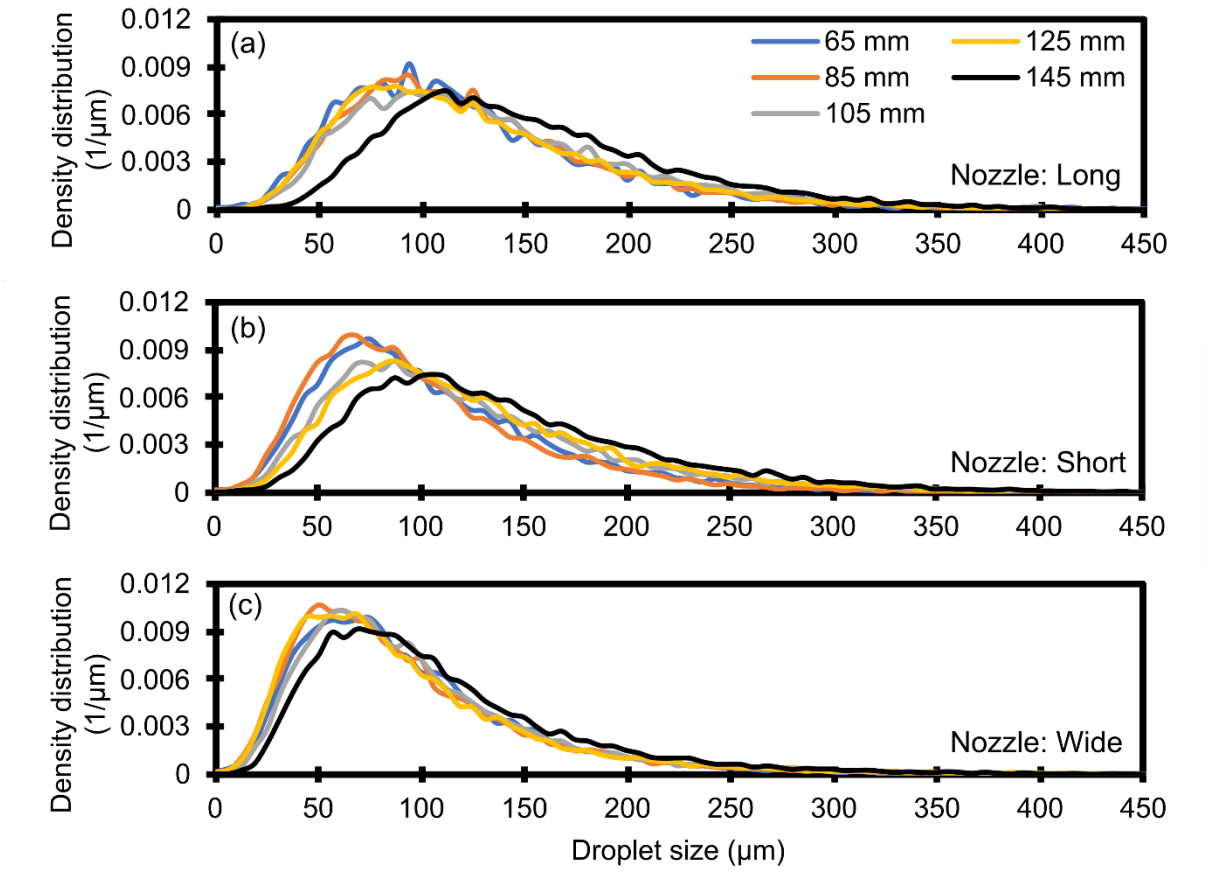

Figure 4. Density distributions of droplet size for different axial positions at the spray centerline for the nozzles (a) Long, (b) Short, and (c) Wide.

The atomization efficiency usually considers only the contribution of the liquid and gas powers to the formation of small droplets, i.e. to the surface effects, rather than the contribution

of the inlet stream's power to the kinetic energy of the droplets. In this regard, following Eq. (1)-(3), the atomization efficiency of each atomizer can be calculated, whose results are shown in **Table 2**. Thus, the overall efficiency between the nozzles indicates a better utilization of the energy provided by the gas and liquid streams for droplet formation by the nozzle Short, with an efficiency of 6.54×10^{-4}. Accordingly, it can be drawn from these analyses that the overall higher atomization efficiencies are induced by shorter internal-mixing chamber lengths. The calculated values agree with the range of efficiencies observed for internal-mixing twin-fluid atomizers reported in the literature [6][11].

Table 2 - Atomization efficiency for each nozzle

Nozzle		
Long	Short	Wide
5.81×10^{-4}	6.54×10^{-4}	6.16×10^{-4}

Conclusions

The Y-jet nozzle is an internal-mixing atomizer widely used industrially, notably in oil refineries, using steam as the dispersing medium. Within this context, the optimization of the nozzle design can improve the spray characteristics matching the necessities of its application.

The investigation of geometrical parameters – the opening angle and length of the mixing chamber - shows a finer spray in the axial direction at the spray center being produced by the shorter internal mixing chamber with the wider opening angle (Wide nozzle). However, although the Wide nozzle directs the air and liquid power toward the droplet surface, producing the smaller droplet sizes, this energy is not transferred as efficiently to the kinetic energy of the liquid, resulting in the lowest velocities among the three nozzles. On the other hand, the Small nozzle is able to produce small droplet sizes (similar to those produced by the Wide nozzle), but with a better distribution of the fluids' power, since the highest spray velocities are also obtained with this nozzle.

The assessment of the spray efficiency shows that the nozzles with shorter mixing chamber lengths have an overall higher efficiency, and among these two geometries (nozzles Short and Wide), the narrower opening angle utilizes the energy provided by the gas and liquid stream to produce small droplets more efficiently.

Therefore, it can be inferred that, within the operating and geometric conditions analyzed in the present study, there is an improvement in spray performance when the internal mixing chamber is shortened and its opening angle is reduced. These statements are based primarily on a higher atomization efficiency obtained with the Short nozzle. In addition, a proper power distribution of the liquid and gas streams to the droplet surface and the kinetic energy of the liquid is observed for this nozzle. This results in the highest velocities and droplet sizes close to the lowest values measured experimentally.

Acknowledgments

Funding for this project has been given with international cooperation between the University of Bremen (GER) and the University of Blumenau (BRA) by means of a PETROBRAS project.

Nomenclature

D_G	Gas inlet port diameter [m]	$p_{G,0}$	Air pressure at atmospheric conditions [Pa]

D_L	Liquid inlet port diameter [m]	$p_{G,abs}$	Absolute gas pressure being injected into the atomizer [Pa]
E_0	Power for driving the liquid and atomizing gas through the nozzle [J s^{-1}]	p_L	Pressure of the liquid being injected into the nozzle [Pa]
E_G	Power necessary to isothermally compress the gas [J s^{-1}]	Q_L	Liquid volumetric flow rate [m^3 s^{-1}]
E_L	Pumping power of the liquid [J s^{-1}]	R	Gas constant [J kg^{-1} K^{-1}]
E_σ	Power to increase the liquid surface energy [J s^{-1}]	SMD	Sauter mean diameter [µm]
GLR	Gas-to-liquid mass flow rate ratio [-]	T	Temperature [K]
$\dot{m}_G$	Air mass flow rate [kg s^{-1}]	σ	Surface tension [N m^{-1}]
PDA	Phase-Doppler anemometer	ϵ	Atomization efficiency [-]

References

[1] Azevedo, C.G., De Andrade, J.C., De Souza Costa, F., 2013. Effects of nozzle exit geometry on spray characteristics of a blurry injector. At. Sprays 23, 193–209. https://doi.org/10.1615/AtomizSpr.2013007244

[2] Barbieri, M.R., Zerwas, A., Utzig, J., França Meier, H., Achelis, L., Fritsching, U., 2021. Drop dynamics and size distribution in a dense spray produced by a twin-fluid atomizer. Int. Conf. Liq. At. Spray Syst. 1. https://doi.org/10.2218/iclass.2021.5804

[3] Barreras, F., Lozano, A., Barroso, J., Lincheta, E., 2006. Experimental characterization of industrial twin-fluid atomizers. At. Sprays 16, 127–145. https://doi.org/10.1615/AtomizSpr.v16.i2.10

[4] Ferreira, G., García, J.A., Barreras, F., Lozano, A., Lincheta, E., 2009. Design optimization of twin-fluid atomizers with an internal mixing chamber for heavy fuel oils. Fuel Process. Technol. 90, 270–278. https://doi.org/10.1016/j.fuproc.2008.09.013

[5] Gao, J., Xu, C., Lin, S., Yang, G., Guo, Y., 2001. Simulations of Gas-Liquid-Solid 3-Phase Flow and Reaction in FCC Riser Reactors. AIChE J. 47, 677–692. https://doi.org/10.1002/aic.690470315

[6] Jedelsky, J., Jicha, M., 2013. Energy conversion during effervescent atomization. Fuel 111, 836–844. https://doi.org/10.1016/j.fuel.2013.03.053

[7] Jolodar, A.J., Akbarnejad, M.M., Taghizadeh, M., Marvast, M.A., 2005. Laser-based flow measurement in performance assessment of FCC atomizer. Chem. Eng. J. 108, 109–115. https://doi.org/10.1016/j.cej.2005.01.009

[8] Kushari, A., 2010. Effect of injector geometry on the performance of an internally mixed liquid atomizer. Fuel Process. Technol. 91, 1650–1654. https://doi.org/10.1016/j.fuproc.2010.06.014

[9] Nazeer, Y.H., Ehmann, M., Koukouvinis, P., Gavaises, M., 2019. The influence of geometrical and operational parameters on internal flow characteristics of internally mixing twin-fluid y-jet atomizers. At. Sprays 29, 403–428. https://doi.org/10.1615/AtomizSpr.2019030944

[10] Pacifico, A.L., Yanagihara, J.I., 2014. The influence of geometrical and operational parameters on Y-jet atomizers performance. J. Brazilian Soc. Mech. Sci. Eng. 36, 13–22. https://doi.org/10.1007/s40430-013-0061-7

[11] Stähle, P., Schuchmann, H.P., Gaukel, V., 2017. Performance and Efficiency of Pressure-Swirl and Twin-Fluid Nozzles Spraying Food Liquids with Varying Viscosity. J. Food Process Eng. 40. https://doi.org/10.1111/jfpe.12317

[12] Zhou, Y., Zhang, M., Yu, J., Zhu, X., Peng, J., 2010. Experimental investigation and model improvement on the atomization performance of single-hole Y-jet nozzle with high liquid flow rate. Powder Technol. 199, 248–255. https://doi.org/10.1016/j.powtec.2010.01.013